Multiply resonant photonic crystal nanocavities for nonlinear frequency conversion

Kelley Rivoire,* Sonia Buckley, and Jelena Vučković

E. L. Ginzton Laboratory, Stanford University, Stanford, California 94305-4085, USA

**krivoire@stanford.edu*

Abstract: We describe a photonic crystal nanocavity with multiple spatially overlapping resonances that can serve as a platform for nonlinear frequency conversion. We show nonlinear characterization of structures with two resonances nearly degenerate in frequency. We also demonstrate structures with resonances separated by up to 523 nm.

OCIS codes: (190.4390) Nonlinear optics, integrated optics; (350.4238) Nanophotonics and photonic crystals; (190.4400) Nonlinear optics, materials; (230.5750) Resonators; (130.3120) Integrated optics devices.

References and links

1. S. Matuso, A. Shinya, T. Kakitsuka, K. Nozaki, T. Segawa, T. Sato, Y. Kawaguchi, and M. Notomi, "High-speed ultracompact buried heterostructure photonic-crystal laser with 13 fJ of energy consumed per bit transmitted," Nat. Photonics **4**, 648–654 (2010).
2. B. Ellis, M. Mayer, G. Shambat, T. Sarmieno, E. Haller, J. Harris, and J. Vučković, "Ultralow-threshold electrically pumped photonic-crystal nanocavity laser," Nat. Photonics **5**, 297–300 (2011).
3. D. Englund, A. Faraon, I. Fushman, N. Stoltz, P. Petroff, and J. Vučković, "Controlling cavity reflectivity with a single quantum dot," Nature **450**, 857–861 (2007).
4. A. Badolato, K. Hennessy, M. Atature, J. Dreiser, E. Hu, P. Petroff, and A. Imamoglu, "Deterministic coupling of single quantum dots to single nanocavity modes," Science **308**, 1158–1161 (2005).
5. B. Song, S. Noda, T. Asano, and Y. Akahane, "Ultrahigh-Q photonic double heterostructure nanocavity," Nat. Mater. **4**, 207–210 (2005).
6. M. Notomi, E. Kuramochi, and H. Taniyama, "Ultrahigh-Q nanocavity with 1D photonic gap," Opt. Express **16**, 11095–11102 (2008).
7. P. B. Deotare, M. W. McCutcheon, I. W. Frank, M. Khan, and M. Lončar, "High quality factor photonic crystal nanobeam cavities," Appl. Phys. Lett. **94**, 121106 (2009).
8. Y. Tanaka, T. Asano, and S. Noda, "Design of photonic crystal nanocavity with Q-factor of $\sim 10^9$," J. Lightwave Technol. **26**, 1532–1539 (2008).
9. A. Rodriguez, M. Soljacic, J. D. Joannopoulos, and S. G. Johnson, "$\chi^{(2)}$ and $\chi^{(3)}$ harmonic generation at a critical power in inhomogeneous doubly resonant cavities," Opt. Express **15**, 7303–7318 (2007).
10. A. Hayat and M. Orenstein, "Photon conversion processes in dispersive microcavities: Quantum-field model," Phys. Rev. A **77**, 013830 (2008).
11. M. Liscidini and L. C. Andreani, "Highly efficient second-harmonic generation in doubly resonant planar microcavities," Appl. Phys. Lett. **85**, 1883–1885 (2004).
12. I. B. Burgess, Y. Zhang, M. W. McCutcheon, A. W. Rodriguez, J. Bravo-Abad, S. G. Johnson, and M. Loncar, "Design of an efficient terahertz sourceusing triply resonant nonlinear photonic crystal cavities," Opt. Express **17**, 20099–20108 (2009).
13. Y. Zhang, M. W. McCutcheon, I. B. Burgess, and M. Loncar, "Ultra-high-Q TE/TM dual-polarized photonic crystal nanocavities," Opt. Lett. **34**, 2694–2696 (2009).
14. M. W. McCutcheon, D. E. Chang, Y. Zhang, M. D. Lukin, and M. Loncar, "Broadband frequency conversion and shaping of single photons emitted from a nonlinear cavity," Opt. Express **17**, 22689–22703 (2009).
15. M. W. McCutcheon, P. B. Deotare, Y. Zhang, and M. Lončar, "High-Q transverse-electric/transverse-magnetic photonic crystal cavities," Appl. Phys. Lett. **98**, 111117 (2011).

#150197 - $15.00 USD Received 29 Jun 2011; revised 4 Aug 2011; accepted 6 Aug 2011; published 24 Oct 2011

16. K. Rivoire, Z. Lin, F. Hatami, W. T. Masselink, and J. Vučković, "Second harmonic generation in gallium phosphide photonic crystal nanocavities with ultralow continuous wave pump power," Opt. Express **17**, 22609–22615 (2009).
17. K. Rivoire, Z. Lin, F. Hatami, and J. Vučković, "Sum-frequency generation in doubly resonant GaP photonic crystal nanocavities," Appl. Phys. Lett. **97**, 043103 (2010).
18. M. W. McCutcheon, J. F. Young, G. W. Rieger, D. Dalacu, S. Frédérick, P. J. Poole, and R. L. Williams, "Experimental demonstration of second-order processes in photonic crystal microcavities at submilliwatt excitation powers," Phys. Rev. B **76**, 245104 (2007).
19. M. W. McCutcheon, G. W. Rieger, I. W. Cheung, J. F. Young, D. Dalacu, S. Frederick, P. J. Poole, G. C. Aers, and R. L. Williams, "Resonant scattering and second-harmonic spectroscopy of planar photonic crystal microcavitites," Appl. Phys. Lett. **87**, 221110 (2005).
20. M. Galli, D. Gerace, K. Welna, T. F. Krauss, L. O'Faolain, G. Guizzetti, and L. C. Andreani, "Low-power continuous-wave generation of visible harmonics in silicon photonic crystal nanocavities," Opt. Express **18**, 26613–26624 (2010).
21. K. Rivoire, S. Buckley, and J. Vučković, "Multiply resonant high quality photonic crystal nanocavities," Appl. Phys. Lett. **99**, to be published (2011).
22. J. Foresi, P. Villeneuve, J. Ferra, E. Thoen, G. Steinmeyer, S. Fan, J. Joannopoulos, L. Kimerling, H. Smith, and E. Ippen, "Photonic-bandgap microcavities in optical waveguides," Nature **390**, 143–145 (1997).
23. M. W. McCutcheon and M. Loncar, "Design of a silicon nitride photonic crystal nanocavity with a quality factor of one million for coupling to a diamond nanocrystal," Opt. Express **16**, 19136–19145 (2008).
24. P. Lalanne, S. Mias, and J. Hugonin, "Two physical mechanisms for boosting the quality factor to cavity volume ratio of photonic crystal microcavities," Opt. Express **12**, 458–467 (2004).
25. C. Sauvan, G. Lecamp, P. Lalanne, and J. Hugonin, "Modal-reflectivity enhancement by geometry tuning in photonic crystal microcavities," Opt. Express **13**, 245–255 (2005).
26. S. Johnson and J. Joannopoulos, "Block-iterative frequency-domain methods for Maxwell's equations in a planewave basis," Opt. Express **8**, 173–190 (2001).
27. S. G. Johnson, C. Manolatou, S. Fan, P. R. Villeneuve, J. D. Joannopoulos, and H. A. Haus, "Elimination of cross talk in waveguide intersections," Opt. Lett. **23**, 1855–1857 (1998).
28. Q. Quan, P. Deotare, and M. Lončar, "Photonic crystal nanocavity strongly coupled to the feeding waveguide," Appl. Phys. Lett. **96**, 203102 (2010).
29. I. Luxmoore, E. Ahmadi, A. Fox, M. Hugues, and M. Skolnick, "Unpolarized H1 photonic crystal nanocavities fabricated by stretched lattice design," Appl. Phys. Lett. **98**, 041101 (2011).
30. O. Benson, C. Santori, M. Pelton, and Y. Yamamoto, "Regulated and entangled photons from a single quantum dot," Phys. Rev. Lett. **84**, 2513–2516 (2000).
31. K. Hennessy, C. Hogerle, E. Hu, A. Badolato, and A. Imamoglu, "Tuning photonic nanocavities by atomic force microscope nano-oxidation," Appl. Phys. Lett. **89**, 041118 (2006).
32. K. Rivoire, A. Faraon, and J. Vučković, "Gallium phosphide photonic crystal nanocavities in the visible," Appl. Phys. Lett. **93**, 063103 (2008).
33. H. Lee, S. Kiravittaya, S. Kumar, J. Plumhof, L. Balet, L. Li, M. Francardi, A. Gerardino, A. Fiore, A. Rastelli, and O. Schmidt, "Local tuning of photonic crystal nanocavity modes by laser-assisted oxidation," Appl. Phys. Lett. **95**, 191109 (2009).
34. A. Faraon and J. Vučković, "Local temperature control of photonic crystal devices via micron-scale electrical heaters," Appl. Phys. Lett. **95**, 043102 (2009).
35. M. Galli, S. Portalupi, M. Belotti, L. Andreani, L. O'Faolain, and T. Krauss, "Light scattering and Fano resonances in high-Q photonic crystal nanocavities," Appl. Phys. Lett. **94**, 071107 (2009).
36. M. Banaee and J. F. Young, "Squeezed state generation in photonic crystal microcavities," Opt. Express **16**, 20908–20919 (2008).
37. W. T. Irvine, K. Hennessy, and D. Bouwmeester, "Strong coupling between single photons in semiconductor microcavities," Phys. Rev. Lett. **96**, 057405 (2006).
38. K. Rivoire, S. Buckley, A. Majumdar, H. Kim, P. M. Petroff, and J. Vučković, "Fast quantum dot single photon source triggered at telecommunications wavelength," Appl. Phys. Lett. **98**, 083105 (2011).
39. D. Englund, D. Fattal, E. Waks, G. Solomon, B. Zhang, T. Nakaoka, Y. Arakawa, Y. Yamamoto, and J. Vučković, "Controlling the spontaneous emission rate of single quantum dots in a 2D photonic crystal," Phys. Rev. Lett. **95**, 013904 (2005).

1. Introduction

Photonic band gap nanocavities confine light into subwavelength volumes with high quality factor, facilitating ultracompact, low-power optoelectronic devices such as lasers [1, 2], as well as studies of fundamental physics such as cavity quantum electrodynamics [3, 4]. State of the art photonic crystal nanocavity designs [5–8] can have quality factors exceeding one million for

#150197 - $15.00 USD Received 29 Jun 2011; revised 4 Aug 2011; accepted 6 Aug 2011; published 24 Oct 2011

a single cavity resonance. For nonlinear optical interactions such as frequency conversion or stimulated Raman scattering, however, it is desirable to have nanostructures that support multiple resonances having arbitrary frequency separation and good spatial field overlap which can be coupled through the nonlinearity of the cavity material. In high quality factor microcavities, the phase matching condition is satisfied by the spatial overlap of the field patterns for each frequency [9–11], allowing high conversion efficiency in a small volume, on-chip device.

In a nanocavity with a single photonic band gap, it is difficult to independently control the frequencies of each mode. Additionally, the field patterns of different modes typically have minimal spatial overlap, and the absolute frequency separation between resonances is limited by the band gap size. Band gaps for different polarizations (e.g. transverse magnetic (TM) and transverse electric (TE)) [12–15] can generate additional resonant modes; however, it is difficult to independently tune their frequencies, and TM resonances require relatively thick membranes that are more difficult to fabricate.

To enable nonlinear coupling of cavity resonances, structures can be fabricated in a III–V semiconductor such as GaP or GaAs (for second or third order optical nonlinearity) or a group IV semiconductor such as silicon (for third order nonlinearities, such as Raman scattering or four wave mixing). Previous experimental work in three and four-wave mixing in semiconductor photonic crystal nanocavities has been implemented using designs featuring a single photonic band gap [16–20]. Recently [21], we proposed a crossed beam photonic crystal cavity suitable for nonlinear frequency conversion that allows at least two individually tunable resonances with a frequency separation larger than the size of the photonic bandgap in a single nanobeam. Here, we extend that work by describing the design as well as experimental linear and nonlinear characterization of structures with resonances that are nearly degenerate with orthogonal polarization, as well as the design and linear characterization of structures with resonances separated by more than 500 nm.

2. Cavity design

An illustration of the design in shown in Fig. 1(a). The basic element of our design is the nanobeam [6, 7, 22–25], a 1D periodic photonic crystal waveguide clad in the other two directions by air, shown in Fig. 1(b). A single unit cell of a single nanobeam, comprising a rectangular airhole with dimensions h_x and h_y in a high index dielectric slab of width w, is shown inside the red box (thickness t of the air-bridged membrane is out of the plane). The structure has periodicity a in the $\hat{x}$ direction; this periodicity produces a 1D TE photonic band gap with size determined by the difference in frequency between the first two bands (dielectric band and air band) at the wavevector $k_x = \pi/a$. We first investigate the periodicities required in a nanobeam structure to achieve different wavelength resonances using 3D simulations performed using plane wave expansion with supercell approach (MIT Photonic Bands (MPB)) [26]. Figure 1(c) plots the wavelengths of the dielectric and air bands obtained from simulations as a function of lattice constant a. Solid lines show wavelengths for fixed absolute thickness of the membrane and are calculated using the refractive index n of GaAs at each wavelength; dotted lines are calculated by scaling the result for wavelength 1550 nm (i.e. fixed t/a, fixed n). Because a real structure has a fixed membrane thickness, decreasing the periodicity in one beam relative to the other leads to larger relative thickness t/a, redshifting the wavelengths of the bands; therefore achieving resonances with relative frequency f_2/f_1 requires superlinear scaling of the feature size, e.g. $a_2/a_1 > f_2/f_1$, as shown by the divergence between solid and dotted lines. (There is a second less important contribution because refractive index increases for higher frequencies, from 3.37 to 3.53 for range plotted in Fig. 1(c)). Figure 1(d) shows the frequencies of dielectric band and air band, as well the relative size of the band gap, as the width of the beam is changed.

The parameters for the crossed beam are shown in Figs. 2(a) and 2(b). A cavity is formed

#150197 - $15.00 USD Received 29 Jun 2011; revised 4 Aug 2011; accepted 6 Aug 2011; published 24 Oct 2011

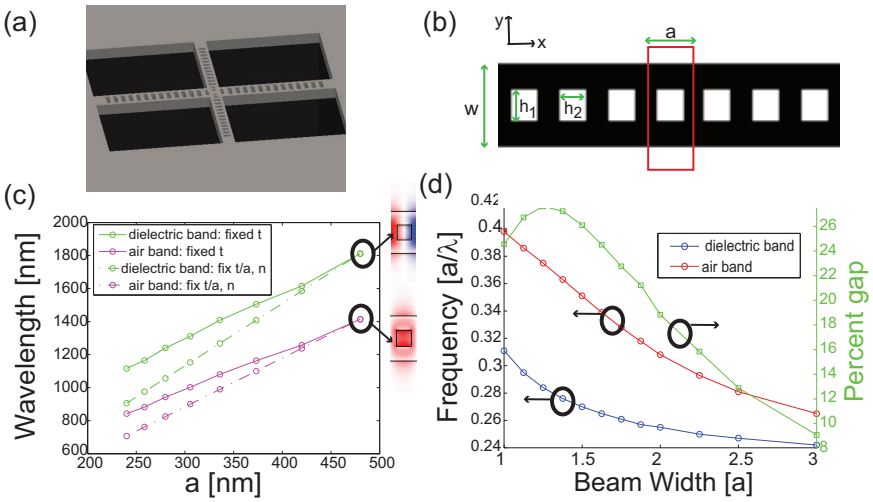

Fig. 1. (a) Schematic illustration of multiply resonant orthogonal nanobeam cavity. (b) Illustration of photonic nanobeam. Red box shows unit cell, which is tiled periodically in the $\hat{x}$ direction. Parameters are periodicity a, width w, hole size h_x and h_y and thickness out-of-plane t (not shown). (c) Wavelengths of dielectric and air bands of GaAs nanobeam as lattice constant is varied. Parameters are w/a=1.65, h_1/w=0.6, h_2/a=0.5. Solid lines are plotted for t=160 nm (fixed absolute slab thickness) and wavelength-dependent index of refraction n; dotted lines are plotted for $t/a = 0.35$ (fixed relative slab thickness) and n=3.37. Field patterns of E_y at $k_x = \pi/a$ for dielectric (top) and air band (bottom) are indicated by black circles and arrows. (d) Normalized frequencies of dielectric and air bands (left axis) of GaAs nanobeam as beam width is varied. Parameters are h_1/w=0.6, h_2/a=0.5, t/a=0.35. Right axis shows change in size of photonic band gap with beam width.

in each beam by introducing a central region with no holes (cavity length l) and tapering the lattice constant and hole size near the cavity region [7,24]. In each beam, confinement along the periodic direction is provided by distributed Bragg reflection; confinement out-of-plane is provided by total internal reflection. Confinement in the in-plane direction orthogonal to the beam axis is provided by total internal reflection, and in the case of beams with overlapping photonic band gaps, also by distributed Bragg reflection [27]. This structure allows nearly independent tuning of each resonant frequency by tuning the parameters (e.g. width, lattice constant, cavity length) of each beam and has natural channels for coupling through each beam to an access waveguide at each wavelength [28]. A cavity with orthogonally polarized resonances degenerate in frequency can be formed by using the same parameters for each beam. This could be used for applications such as coupling to spin states of embedded quantum emitters [29] or for building polarizaton entangled photon sources based on a bi-excitonic cascade from a single quantum dot [30, 31]. Figures 2(c) and 2(d) show the field patterns from 3D finite difference time domain (FDTD) simulations for a doubly degenerate structure. The cavities also have several additional higher order modes the number of which is determined primarily by cavity length (two per beam for the structures shown in Fig. 2) with additional field pattern nodes.

#150197 - $15.00 USD Received 29 Jun 2011; revised 4 Aug 2011; accepted 6 Aug 2011; published 24 Oct 2011

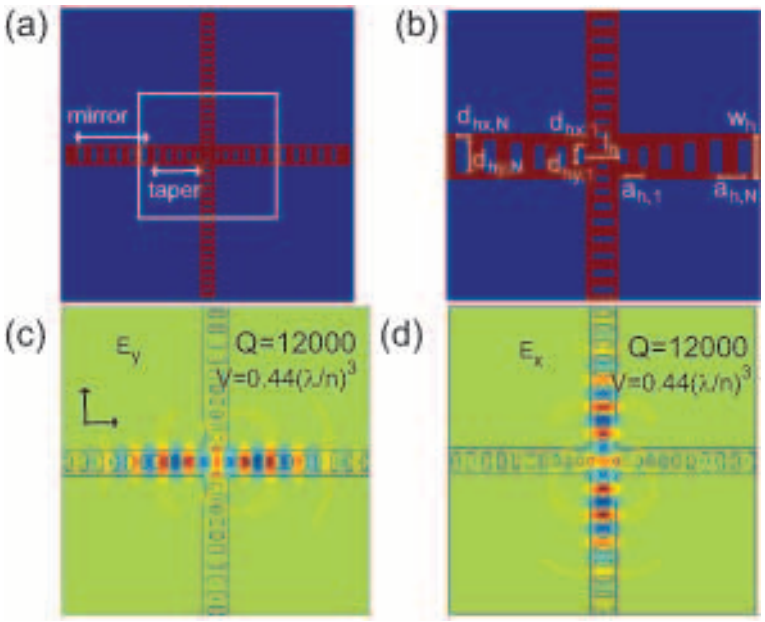

Fig. 2. (a) Crossed nanobeam cavity design, showing intersecting orthogonal nanobeams with taper and mirror regions, as well as central cavity. (b) Detail of white box in (a). Parameters used to form resonance, shown for cavity in horizontal (subscript h) beam: l_h indicates cavity length; $d_{hx,N}$ and $d_{hy,N}$ indicate hole sizes in mirror region; $d_{hx,1}$ and $d_{hy,1}$ indicate hole sizes in first taper period; $a_{h,N}$ indicates periodicity in mirror region; $a_{h,1}$ indicates periodicity in first taper period, w_h indicates beam width. The corresponding parameters are similarly introduced for the vertical beam (with subscript v). The thickness of both beams (in the z direction) is t. Parameters are changed linearly inside the taper. (c) 3D FDTD simulation of field pattern of E_y for cavity localized in horizontal beam by tapering hole dimensions and lattice constant in central region. Parameters are: $a_{h,N} = a_{v,N}$=449 nm, $d_{hx,1}/d_{hx,N} = d_{hy,1}/d_{hy,N}$=0.5, $a_{h,1}/a_{h,N} = a_{v,1}/a_{v,N}$=0.7, $l_h/a_{h,N} = l_v/a_{v,N} = 1.4$, $w_h/a_{h,N} = w_v/a_{v,N}$=1.65, $d_{hy,N}/w_h = d_{vx,N}/w_v$=0.7, $d_{hx,N}/a_h = d_{vy,N}/a_{v,N}$=0.5, refractive index $n = 3.37$, with slab thickness $t/a_{h,N}$=0.35, N=8, and 6 mirror periods for both beams. Resonant wavelength is 1.55 μm with Q=12,000 and V=0.44$(\lambda/n)^3$. (d) Field pattern of E_x for cavity localized in vertical beam. Parameters are same as in (c).

3. Linear and nonlinear spectroscopy of cavities with nearly degenerate resonant frequencies

We now present linear nonlinear characterization of cavities with nearly degenerate resonant frequencies. A scanning electron microscope (SEM) image of structure fabricated in GaAs is shown in Fig. 3(a). The structures are defined by e-beam lithography and dry etching, as well as wet etching of a sacrificial AlGaAs layer underneath the 164 nm thick GaAs membrane. To characterize the resonant frequencies of the structures, we measure reflectivity, using vertical incidence through an objective lens and free space coupling, in the cross-polarized configuration using a tungsten halogen lamp as a broadband light source [32]. The principle of the measurement is illustrated in Fig. 3(b). The input and measurement polarizations are orthogonal; the cavity polarization is oriented 45 degrees to both output and input. The cavity acts as a frequency-selective polarization rotator, filtering light at the frequencies of the cavity resonances, resulting in a high-signal to noise measurement of the cavity reflectivity from which

#150197 - $15.00 USD Received 29 Jun 2011; revised 4 Aug 2011; accepted 6 Aug 2011; published 24 Oct 2011

the quality factor can be extracted. The result of this measurement for the structure in Fig. 3(a) is shown in Fig. 3(c). There are two resonances visible at 1571.2 nm (Q=4700) and 1573.9 nm (Q=7200). The difference between the frequencies of the resonances is due to fabrication imperfections; improving fabrication or employing local tuning [31,33,34] could assist in yielding perfectly degenerate resonances. Quality factors are extracted by fitting the measured data to the sum of two Fano lineshapes [35], plus linear background (to account for the measured background from the white light source).

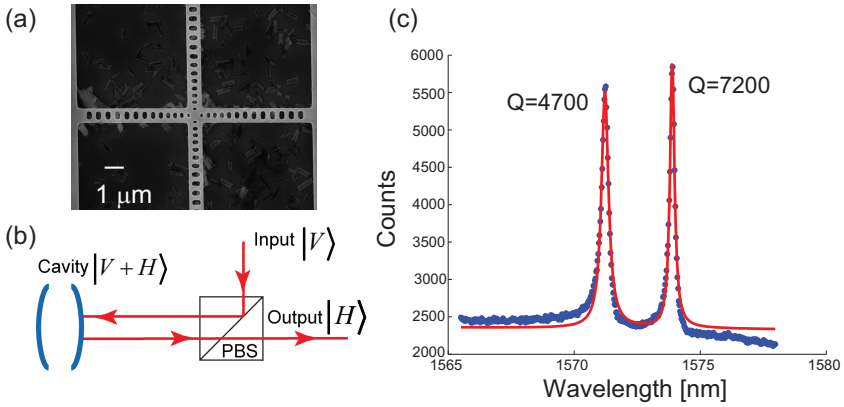

Fig. 3. (a) Scanning electron microscope image of crossbeam structures with identical parameters in both beams. Structures are fabricated by e-beam lithography, dry etching, and wet etching. (b) Experimental setup for cross-polarized reflectivity measurements to characterize cavity resonances. PBS indicates polarizing beamsplitter. Cavity polarization is oriented 45 degrees ($|H+V\rangle$) from orthogonal input ($|V\rangle$) and measurement ($|H\rangle$) polarizations. (c) Cross-polarized reflectivity measurement of structure in (a), showing two resonances at 1571.2 nm (Q=4700) and 1573.9 nm (Q=7200). Solid line indicates fit to sum of two Fano lineshapes.

This cross-polarized configuration, however, cannot easily distinguish between cavities with vertical and horizontal polarizations, and also cannot resolve resonances with frequencies separated by less than a linewidth. To more sensitively measure cavity resonances, we use intracavity second harmonic generation [16, 19]. This allows us to absolutely determine the far-field polarization of the cavity, since second harmonic generation is maximized when incident light is aligned to the polarization of the cavity. Additionally, because the measured lineshape from the second harmonic is proportional to the square of the lineshape from the cavity, we can more easily distinguish cavities separated by small differences in frequency. A second harmonic measurement of a different structure with nearly degenerate resonances in shown in Fig. 4. Figure 4(a) shows the second harmonic counts measured for three different incident laser polarizations as the laser wavelength is varied. The angle of alignment between input polarization and the polarization of each cavity mode determines the fraction of power coupled into the cavity, and accordingly affects the magnitude of second harmonic generated. The intensity of second harmonic generation for each mode also depends on the free space coupling efficiency, quality factor of the mode, spatial overlap of fundamental and second harmonic fields, and detuning of laser wavelength from the cavity resonance [16]. Two modes with orthogonal polarization (with resonant wavelengths 1541.75 nm and 1542.1 nm), as expected, are clearly visible. To further illustrate this, we scan additional incident polarizations and wavelengths, as shown in Figs. 4(b) and 4(c). Figure 4(c) shows 2D slices at three incident laser wavelengths. The red

#150197 - $15.00 USD Received 29 Jun 2011; revised 4 Aug 2011; accepted 6 Aug 2011; published 24 Oct 2011

lines show fits for two resonances with polarization separated by exactly 90 degrees, in good agreement with the measured data.

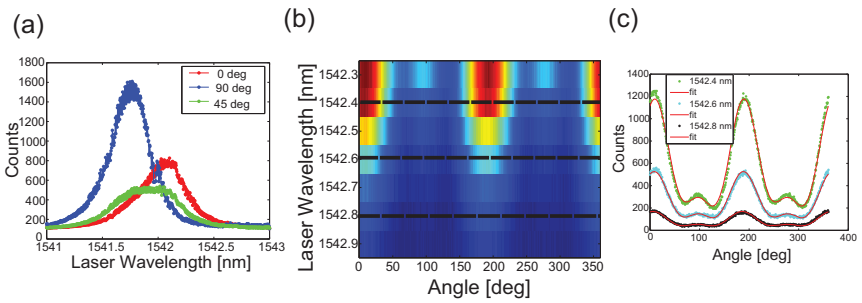

Fig. 4. (a) Second harmonic characterization of structure with two resonances nearly degenerate in frequency as a function of laser wavelength for 3 polarizations. Two modes with orthogonal polarization are visible. (b) Second harmonic intensity as a function of incident laser polarization. Vertical axis indicates wavelength of laser; horizontal axis indicates angle of polarization. Color indicates second harmonic intensity. Dotted horizontal lines indicate traces in (c). (c) Line plots of second harmonic generation measured at different polarizations for three laser wavelengths shown in (b). Red lines indicate fits for two cavity modes with polarizations separated by exactly 90 degrees.

We also perform nonlinear mixing with two resonant modes detuned in frequency. Figure 5 shows sum-frequency generation performed in a structure with resonances at 1552.8 nm and 1558.9 nm (selected to have two resonances overlapping with the high power range of our tunable lasers and large enough frequency separation to observe the SFG peak). The central sum-frequency peak is smaller due to the smaller spatial overlap between the two modes than with a single mode. There is no cavity resonance at either the second harmonic or sum frequency.

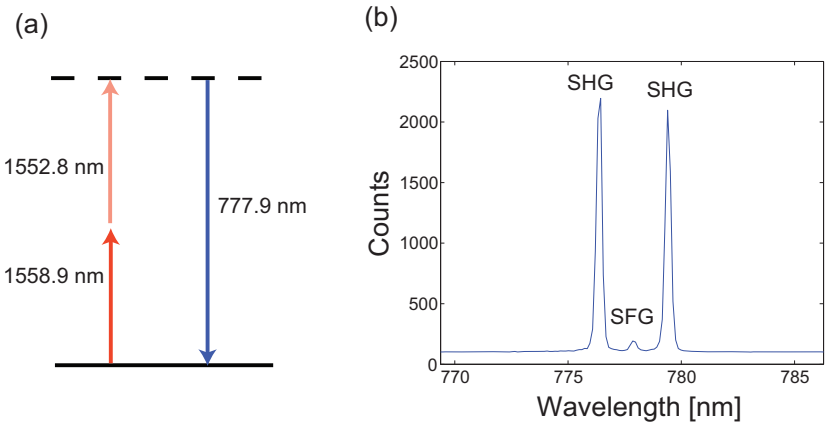

Fig. 5. (a) Schematic of sum frequency generation. Light from two CW lasers is coupled into two cavity resonances at 1552.8 nm and 1558.9 nm. Nonlinear frequency conversion produces light at the second harmonic frequencies of each laser, as well as at the sum frequency, 777.9 nm. (b) Sum-frequency generation from structure with resonances as indicated in (a).

#150197 - $15.00 USD Received 29 Jun 2011; revised 4 Aug 2011; accepted 6 Aug 2011; published 24 Oct 2011

4. Multiple resonances with large frequency separation

To create nonlinear optical sources at arbitrary wavelengths, it is also desirable to design the cavity to have large separation between cavity resonances. Figures 6(a) and 6(b) show simulated cavity fields for structures with resonances at 1.55 μm and 1.103 μm. The maximum separation in frequency that can be achieved is related to the ratio of the two beam widths, as the quality factor of the higher frequency mode is limited by diffraction into the orthogonal beam (Fig. 6(c)) as the difference between the beam widths grows (arbitrarily increasing the beam width for a fixed lattice constant would decrease the size of the photonic band gap and reduce the mode quality factor, as shown in Fig. 1(d)). The quality factor is limited for both resonances by out-of-plane scattering. An SEM of a fabricated structure with resonances separated by a large frequency difference is shown in Fig. 6(d).

For nonlinear frequency conversion applications, it is important for cavity field patterns to have large spatial overlap. Defining the nonlinear overlap, normalized to 1, as [13]

$$\gamma \equiv \frac{\varepsilon_{NL} \int_{NL} dV \sum_{i,j,i\neq j} E_{1,i} E_{2,j}}{\sqrt{\int dV \varepsilon |E_1|^2} \sqrt{\int dV \varepsilon |E_2|^2}} \tag{1}$$

where *NL* indicates nonlinear material only, we calculate γ=0.02 for the structures shown in Fig. 6. This number could be increased to 0.07 by decreasing the number of taper periods from 5 to 3; the quality factors are reduced to 1440 and 1077 respectively, although this could likely be increased by reoptimization of other parameters. The value of γ for the degenerate cavity presented earlier is also 0.02. The value of γ for a single resonance of the degenerate structure overlapped with itself is 0.89 (i.e. γ is determined by the fraction of field in the nonlinear material), indicating the size of γ is limited by the amount of field concentrated in the central region. This overlap is smaller than that for TE_{00} and TM_{00} modes in a single nanobeam [13]; however, our design uses a thinner membrane which is easier to fabricate and can support larger frequency separations.

Figure 7 shows cross-polarized reflectivity measurements using a broadband source of structures with resonances at 1546.6 nm (Q=1600) and 1023 nm (Q=500), a frequency separation of 523.6 nm. We believe the experimental Q factors are limited by fabrication inaccuracies caused by the small feature size of the central holes in the vertical beam, which are located in regions of high field for both resonances. We could not perform nonlinear characterization of these structures due to lack of availability of a laser at 1023 nm.

5. Improving the crossbeam frequency conversion platform

For highly efficient three wave mixing, it would be desirable to have all three frequencies confined by cavity modes. This could be achieved by additionally using a higher order mode in one beam. However, all cavity resonances in our design have electric field primarily in plane (TE), while nonlinear frequency conversion in III-V semiconductors grown on (100)-oriented wafers requires at least one frequency to have out of plane (TM) polarization (because the only non-zero elements of the bulk $\chi^{(2)}_{ijk}$ have $i \neq j \neq k$ [16]). This can be circumvented by using a wafer with different crystal orientation such as (111) [36, 37] so that the effective $\chi^{(2)}$ tensor is rotated to have more non-zero elements. Figure 8 shows a concept illustration of highly efficient doubly resonant second harmonic generation using the crossbeam structure.

Our design is also interesting for integration with single semiconductor emitters, which is important for creating quantum photonic interfaces between different quantum emitters and telecommunications wavelength. Recently [38], we demonstrated second harmonic excitation of a InAs single quantum dot emitting at 900 nm, creating a fast single photon source triggered at telecommunication wavelengths (triggered single photons at 100 MHz, with nonclassical

#150197 - $15.00 USD Received 29 Jun 2011; revised 4 Aug 2011; accepted 6 Aug 2011; published 24 Oct 2011

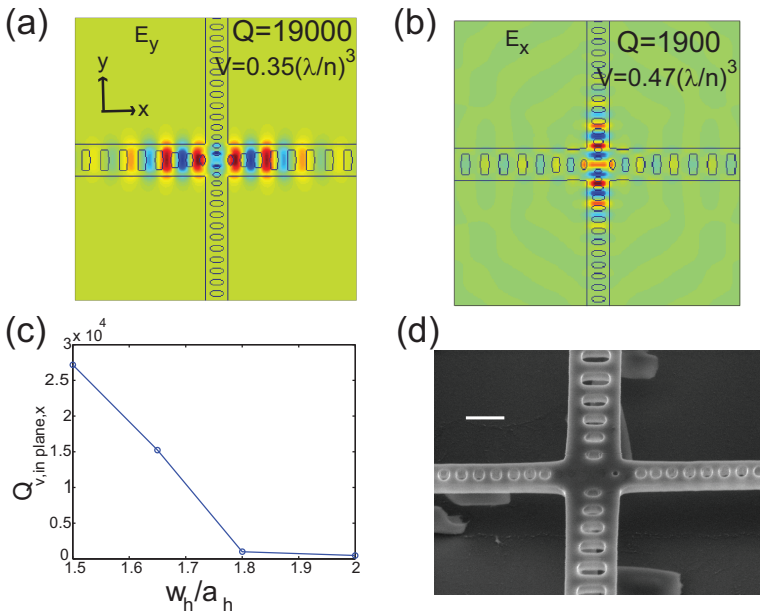

Fig. 6. (a) Field pattern of E_y for cavity localized in horizontal beam by tapering hole dimensions and lattice constant in central region. Parameters are: $a_{h,N}$=453 nm, $a_{v,N}$=272 nm, $d_{hx,1}/d_{hx,N} = d_{hy,1}/d_{hy,N}$=0.5, $a_{h,1}/a_{h,N} = a_{v,1}/a_{v,N}$=0.7, $l_h/a_{h,N} = 1.2$, $l_v/a_{v,N}$=0.83, $w_h/a_{h,N}$=1.65, $w_v/a_{v,N}$=1.8, $d_{hy,N}/w_h = d_{vx,N}/w_v$=0.7, $d_{hx,N}/a_h = d_{vy,N}/a_{v,N}$=0.5, refractive index $n = 3.37$, with slab thickness $t/a_{h,N}$=0.35, N=5, and 6 mirror periods for both beams. Resonant wavelength is 1.55 μm with Q=19,000 and V=0.35$(\lambda/n)^3$. (b) Field pattern of E_x for cavity localized in vertical beam. Resonant wavelength is 1103 nm with Q=1900 and V=0.47$(\lambda/n)^3$. (c) Change in in-plane quality factor in $\hat{x}$ direction (i.e. radiated power collected at x and -x edges of simulation space) for resonance localized by vertical beam as a function of w_h. (d) Tilted SEM of the fabricated structure. Scale bar corresponds to 1 μm.

statistics visible at 300 MHz) . The speed of that source could be improved by using a second cavity resonance, as in our crossed beam design, to enhance the spontaneous emission rate of the quantum dot through the Purcell effect [39], with possible speeds exceeding 1 GHz. Finally, our design is also promising for intracavity frequency conversion of single photons from an integrated quantum emitter [14].

6. Conclusions

In summary, we describe a crossed nanobeam platform for nonlinear frequency conversion that allows small mode volume cavities with spatial overlap and large frequency separation. We demonstrate cavities with nearly-degenerate frequencies, as well as frequencies separated by more than 500 nm, which we characterize by linear and nonlinear spectroscopy. Finally, we propose extensions of this work to allow high efficiency frequency conversion, which might be used in conjunction with integrated single emitters.

#150197 - $15.00 USD Received 29 Jun 2011; revised 4 Aug 2011; accepted 6 Aug 2011; published 24 Oct 2011

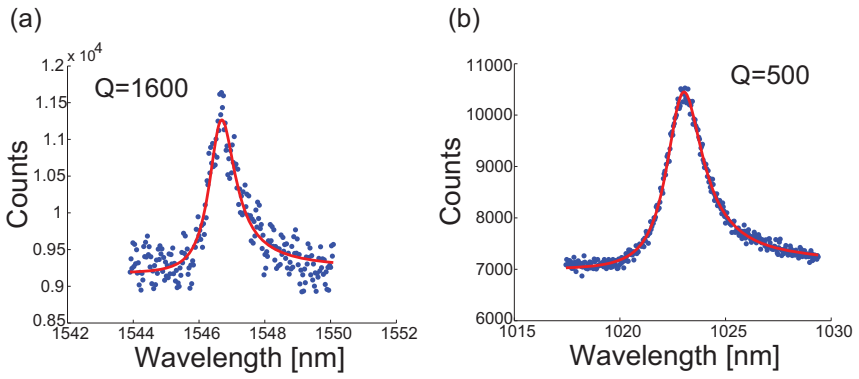

Fig. 7. Cross-polarized reflectivity of crossbeam structure with resonances separated by 523 nm. (a) Resonance at 1546.6 nm (Q=1600). (b) Resonance at 1023 nm (Q=500).

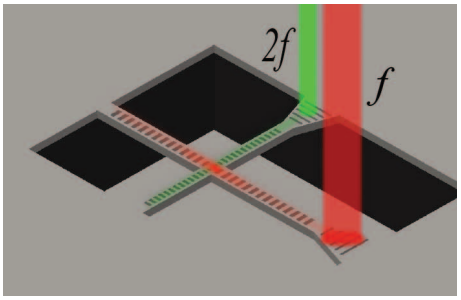

Fig. 8. Concept illustration of doubly resonant second harmonic generation in photonic crystal crossbeam nanocavity. Incident light (red) is coupled into the structure via a grating, transmitted to the cavity, frequency converted, and outcoupled through a separate grating (green).

Acknowledgments

Financial support was provided by the National Science Foundation (NSF Grant ECCS-10 25811). KR and SB supported by Stanford Graduate Fellowships and the NSF GRFP (SB). This work was performed in part at the Stanford Nanofabrication Facility of NNIN supported by the National Science Foundation under Grant No. ECS-9731293.

#150197 - $15.00 USD Received 29 Jun 2011; revised 4 Aug 2011; accepted 6 Aug 2011; published 24 Oct 2011